INSTITUTE OF PHYSICS PUBLISHING JOURNAL OF PHYSICS: CONDENSED MATTER

J. Phys.: Condens. Matter **13** (2001) 5875–5891 www.iop.org/Journals/cm PII: S0953-8984(01)24141-1

Periodic structures induced by normal-incidence sputtering on Ag(110) and Ag(001): flux and temperature dependence

G Costantini[1], S Rusponi[2], F Buatier de Mongeot, C Boragno and U Valbusa

INFM—Unità di Ricerca di Genova, Centro CFSBT-CNR and Dipartimento di Fisica, Via Dodecaneso 33, I-16146 Genova, Italy

Received 20 April 2001, in final form 4 June 2001

Abstract

The morphology generated on Ag(110) and Ag(001) by 1 keV Ar^+ sputtering at normal incidence has been studied by scanning tunnelling microscopy as a function of the substrate temperature T_S and the ion flux Φ. Since ion sputtering is a non-equilibrium process in which erosion competes with diffusion in determining the surface evolution, these macroscopic parameters can be used to tune the final surface morphology. Flat or rough surfaces as well as periodic structures have been observed on both substrates. On Ag(110), ion sputtering at 230 K and 320 K produces two well defined ripple patterns whose wave vectors are parallel to $\langle 1\bar{1}0\rangle$ and $\langle 001\rangle$ respectively, while on Ag(001) a periodic pattern of square islands has been observed over a wide range of substrate temperatures ($240\ \mathrm{K} \leqslant T_S < 440\ \mathrm{K}$). Similar to the results reported in growth experiments, a flux increase produces a surface evolution qualitatively comparable with that obtained by lowering the temperature. The results are discussed in terms of a continuum model for the ion sputtering process.

1. Introduction

The evolution of the surface morphology during ion sputtering is a complex phenomenon which involves roughening and smoothing processes. Experimental studies on amorphous [1, 2] and semiconductor materials [3–5] show that off-normal ion sputtering at room temperature generates a periodic modulation of the surface (ripples). Depending on the ion incidence angle θ, the ripple wave vector $\boldsymbol{k}$ can be either perpendicular (θ close to grazing) or parallel (θ close to normal) to the projection of the ion beam in the surface plane. These results have

[1] Present address: Max-Planck-Institut für Festkörperforschung, Heisenbergstraße 1, D-70569 Stuttgart, Germany.
[2] Present address: Institut de Physique Expérimentale, Ecole Polytechnique Fédérale de Lausanne, CH-1015 Lausanne, Switzerland.

0953-8984/01/265875+17$30.00

been theoretically explained in terms of a linear instability caused by the surface-curvature-dependent sputtering yield, which competes with and dominates the smoothing due to thermal surface diffusion [6, 7]. In contrast, for near-to-normal incidence ($\theta \cong 0^\circ$), no periodic structures are observed since the smoothing effect, due to the diffusion of the recoiling atoms induced by irradiation, dominates the erosion instability [8].

For single-crystal metals the scenario is quite different. Ion sputtering under similar experimental conditions produces well defined periodic features that reflect the symmetry of the substrate without any relation with the ion beam direction: square pits have been observed on Cu(001) [9] and Ag(001) [10], hexagonal ones on Pt(111) [11], Au(111) [12] and Cu(111) [13].

Moreover, in a recent paper [14], a ripple structure whose wave vector $\boldsymbol{k}$, depending on the substrate temperature, is parallel to $\langle 1\bar{1}0\rangle$ or $\langle 001\rangle$ has been observed on Cu(110) following sputtering at normal incidence. This result has been explained as a joint effect of the Schwoebel barrier on inter-layer diffusion and the anisotropic intra-layer mobility which characterizes the surface. In fact, as shown by the authors, a Schwoebel barrier, limiting the inter-layer mass transport, generates a further ripple instability which can overcome the one due to ion erosion. Since on a Cu(110) surface diffusion is anisotropic, the substrate temperature can be varied in order to select along which of the two crystallographic directions the effect of the Schwoebel barrier is activated and therefore to select the orientation of the ripples. A similar explanation has recently been suggested by Ramana Murty *et al* [12] to describe the pit coarsening observed during Au(111) ion sputtering.

In order to verify the general validity of this picture, we have carried out a comparative study of the Ag(110) and Ag(001) surface evolution induced by normal sputtering ($\theta \cong 0^\circ$) as a function of the substrate temperature T_S. Since, on Ag(110), surface diffusion is anisotropic while it is isotropic on Ag(001), a comparison of the results on these two surfaces should help to shed light on the phenomenon under investigation. The data on Ag(110) show that, similarly to what was observed on Cu(110) [14], ion sputtering produces a ripple pattern whose wave vector turns from $\langle 1\bar{1}0\rangle$ to $\langle 001\rangle$ on increasing the substrate temperature (ripple rotation). On the other hand, ion sputtering on Ag(001), for which surface diffusion is isotropic, generates only a periodic pattern of square pits.

In addition to the temperature evolution we have also studied the dependence of the surface morphology on the ion flux. Since ion sputtering is a non-equilibrium process in which erosion competes with surface diffusion in determining the final surface structure, the surface evolutions obtained by varying the ion flux at a fixed temperature or by varying the temperature at a constant ion flux should be similar. In fact, periodic structures can be produced only if the sputtered surface is able to reorganize itself between one ion hit and the following one, through the diffusion of adatoms and vacancies. Therefore, lowering the temperature, and thus depressing the diffusion, has the same effect as increasing the ion flux and thus reducing the time interval between successive ion hits. In agreement with this picture, the experimental data show that on Ag(110) an increase of the ion flux Φ, at a fixed substrate temperature, produces a rotation of the surface periodicity, similar to that observed on lowering the substrate temperature at a fixed erosion rate. A similar parallelism between high-flux and low-temperature behaviour is reported also for on Ag(001).

The paper is organized as follows. In section 2 we present the experimental details. Section 3 contains a description of the parameters that we employ to characterize the surface morphology, i.e. the surface roughness and coherence of the observed periodic structures. The experimental results are described in section 4, while their discussion in terms of the continuum equations recently proposed by Cuerno and Barabasi [7] and Rusponi *et al* [14] is developed in section 5. Finally, a summary and conclusions are given in section 6.

2. Experiment

The experiments were carried out by means of a variable-temperature STM, located in an ultrahigh-vacuum chamber (base pressure 1×10^{-10} mbar) equipped with standard facilities. The most relevant feature of this system is the possibility it affords of performing all the necessary sample preparations, included annealing and sputtering, and the subsequent measurements without any sample transfer, so that the sample temperature is continuously monitored and kept at a desired value [15]. The surface has been prepared by several cycles of 1 keV Ar^+ sputtering at 350 K, followed by flash annealing up to 750 K and 850 K respectively in the cases of Ag(110) and Ag(001). Since the crystals are aligned to better than 0.2° respectively along the (110) and (001) planes, the resulting terraces show characteristic extensions close to 600 Å. In figure 1 we show the Ag(001) surface after the preparation procedure and, in the inset, the resolved atomic structure. The experiments consist in sputtering the crystal surface with 1 keV Ar^+ ions, for different values of the ion flux Φ (evaluated from the ion current collected on the sample), sputtering time t, incidence angle θ and azimuth angle δ (figure 2), at a temperature T_S variable over the range 100–500 K. After sputtering, the sample is frozen at $T \approx 100$ K in order to inhibit subsequent surface reorganization. In the finite time necessary to quench the sample (less than 5 min), the surface morphology undergoes only minor modifications. In fact, as we noted in a previous work [16], the relaxation time of the Ag(110) surface, which, because of the lower energy barriers, is even more 'mobile' than Ag(001), is very long (some hours) even at room temperature, since surface relaxation requires adatom step detachment which is a process with a very high activation energy barrier [17]. In this paper we limit the discussion to just the results obtained by normal sputtering ($\theta = 0°$), where the experimental geometry is invariant for azimuthal rotation. In all the experiments the tunnelling parameters are characterized by a tip–sample voltage in the 1–1.5 V range, while the tunnelling current is about 1 nA. Under these conditions, the effect of scanning on the sample

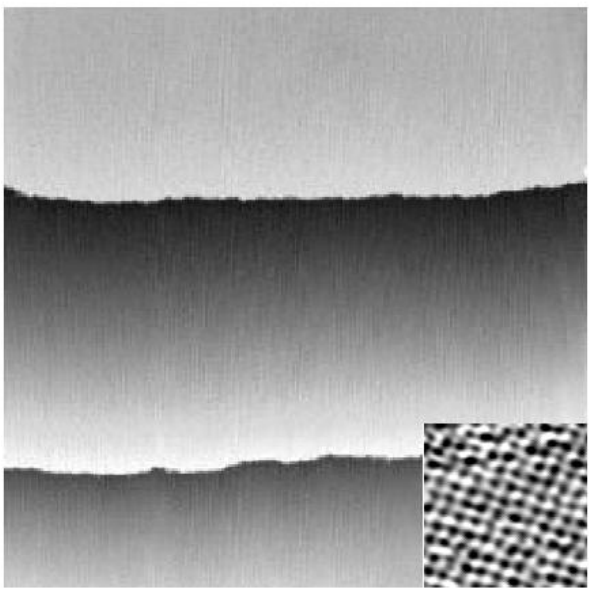

Figure 1. Ag(001) after several sputtering and annealing cycles. Large terraces develop on the surface (image size 350×350 nm^2). In the inset the atomic structure is resolved.

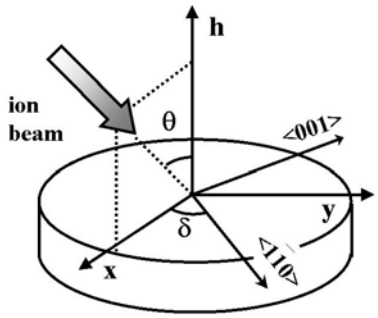

Figure 2. A schematic view of the experimental geometry. (x, y, h) represents the laboratory frame, h is the normal to the flat surface, while the x–h plane is defined by the ion trajectories. Our experimental results refer to the case in which $\theta = 0^\circ$. In this situation the experimental geometry is invariant for azimuthal rotation and therefore we can assume $\delta = 0^\circ$.

morphology is negligible, as directly observed by comparing subsequent images. Images have been acquired both in the derivative mode, in order to enhance the contrast and to offer a better view of the surface morphology, and in the absolute mode, which is necessary to characterize quantitatively the different topographies.

3. Analysis

We characterized the evolution of the surface morphology in terms of the *surface roughness* W and the *coherence* C of the periodic structure. These quantities are estimated from the discrete 2D-autocorrelation function $G(i, j) = \langle h(i, j)h(i', j')\rangle$ where $h(i, j)$ is the surface height at site (i, j). We evaluated $G(i, j)$ over a large number of STM topographies recorded as 512×512 numerical matrices. Since experimental data may be affected by an instrument-induced overall slope that could alter the measured $G(i, j)$ value, we subtracted the best-fit plane from the raw data pixel by pixel. If $h(i, j)$ represents the measured surface height at sampling point (i, j) and $\bar{h}(i, j)$ is the local value of the fitting plane, one can calculate the corrected discrete 2D-autocorrelation function:

$$G(i, j) = \frac{1}{L^2}\sum_{n,m}[h(i+n, j+m) - \bar{h}(i+n, j+m)][h(i, j) - \bar{h}(i, j)]$$

as the inverse discrete Fourier transform of the power spectrum $P(k, l) = \hat{h}(-k, -l)\hat{h}(k, l)$ where $\hat{h}(k, l)$ is the discrete Fourier transform of the corrected surface height $h(i, j) - \bar{h}(i, j)$ [18, 19]. The roughness is then defined by the relation $W = (1/2)\sqrt{G(0, 0)}$ [20] and, by definition, it represents a measure of the total surface corrugation.

In order to characterize and give prominence to the presence of surface modulations, we computed the *coherence* C. We defined C by taking linear sections of the 2D-autocorrelation function and computed the ratio of the height of the first secondary maximum versus the height of the central peak (both heights normalized with respect to the first minimum) (figure 3). By definition, the value of C can vary over the range $0 \leqslant C \leqslant 1$. $C = 1$ indicates a perfect periodic surface modulation with the crests perpendicular to the sampling direction, while $C = 0$ indicates the absence of correlation. Thus the value of C allows one to determine whether or not a surface is periodic in a fixed direction. The STM topography of an Ag(110) sputtered surface shows the presence of ripple structures with the wave vector $\boldsymbol{k}$ aligned with $\langle 001\rangle$ or $\langle 1\bar{1}0\rangle$, depending on the sputtering conditions. For this reason we estimated C both

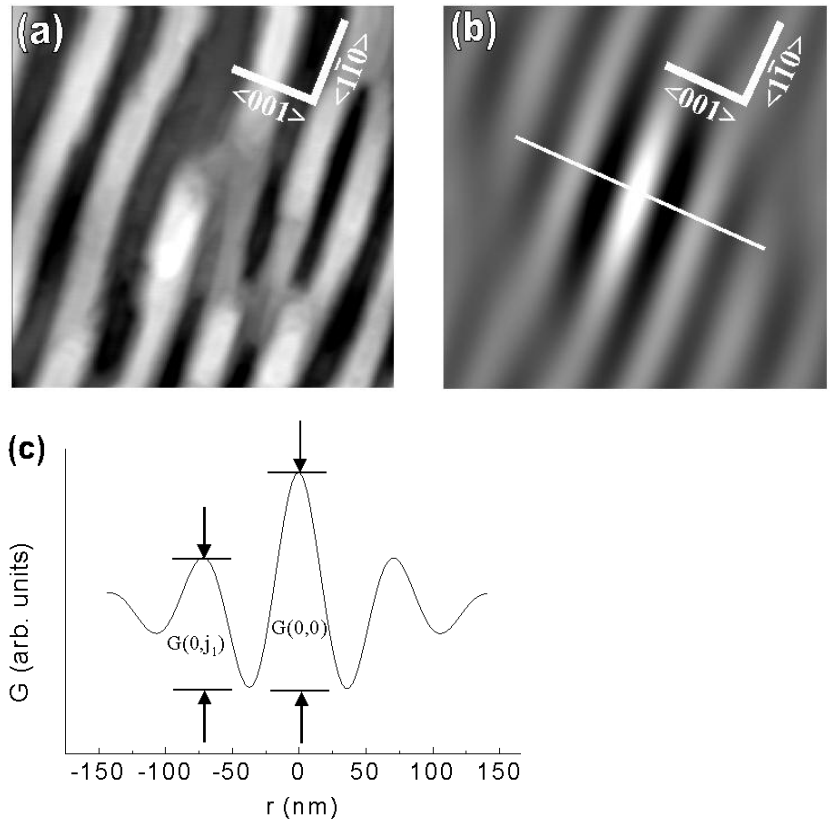

Figure 3. (a) Typical STM topography (size 400 × 400 nm^2) after ion sputtering on Ag(110) at $T_S = 320$ K, $\Phi = 4$ μA cm^{-2}, $t = 15$ min. (b) The corresponding 2D-autocorrelation function. (c) An example of a linear section along the marked line in (b) which corresponds to a ⟨001⟩ crystallographic direction. The value of the *coherence C* along ⟨001⟩ is defined as $C_{001} = G(0, j_1)/G(0, 0)$ where $(0, j_1)$ is the position of the first secondary maximum along ⟨001⟩.

along ⟨001⟩, in the following referred to as C_{001}, and along ⟨1$\bar{1}$0⟩, in the following referred to as $C_{1\bar{1}0}$. In the case of Ag(001), since the surface morphology is symmetric along its two principal crystallographic directions, this distinction is not necessary.

4. Results

We have separately studied the effects of erosion and diffusion on the final surface morphology. Fixing the erosion rate, i.e. the ion flux Φ, the substrate temperature can be changed in order to activate different diffusion processes. Figure 4 shows the Ag(110) surface topography resulting after sputtering at $\Phi = 4$ μA cm^{-2} for different values of T_S. At the lowest temperature considered ($T_S = 180$ K) the surface is almost uniformly rough (figure 4(a)). For T_S in the range 230–270 K, the surface is characterized by a well defined ripple structure (wavelength $\simeq$ 15 nm) with the crests aligned along ⟨001⟩ (wave vector along ⟨1$\bar{1}$0⟩; figure 4(b)). A little increase in the sputtering temperature ($280 \leqslant T_S \leqslant 290$ K) produces a degradation of this structure and the surface displays a pattern of pits and mounds (figure 4(c)). Although their distribution is affected by a certain amount of randomness, it is clear that

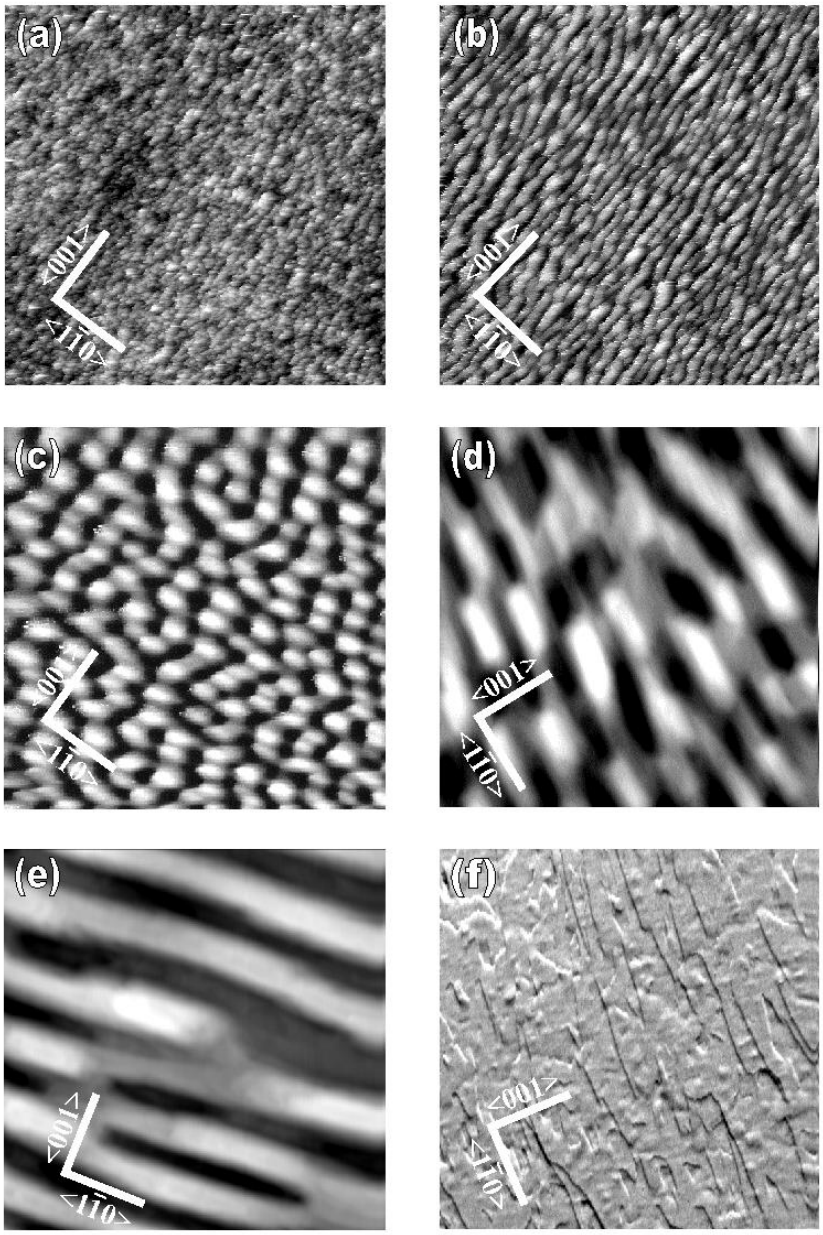

Figure 4. Six images (size 400 × 400 nm^2) of Ag(110) after ion sputtering ($\Phi = 4$ μA cm^{-2}, $t = 15$ min) at normal incidence ($\theta = 0^\circ$) for different temperatures. (a) $T_S = 180$ K; (b) 230 K; (c) 280 K; (d) 300 K; (e) 320 K; (f) 350 K. Image (f) has been acquired in derivative mode and thus appears as if illuminated from the right-hand side.

they originate from the superposition of two perpendicular ripple patterns: the first with the crests oriented along $\langle 001 \rangle$, thus similar to that observed at lower temperatures, and a second new one oriented along $\langle 1\bar{1}0 \rangle$. A further increase of T_S ($T_S \cong 300$ K) brings about a gradual disappearance of the first ripple structure and a simultaneous increase of

the second one (figure 4(d)), until, for $T_S \cong 320$ K, only one well developed periodic pattern (wavelength $\cong 60$ nm) with the crests along $\langle 1\bar{1}0\rangle$ is observable (90° ripple rotation) (figure 4(e)). Finally, at higher temperatures, a quasi-layer-by-layer erosion is observed (figure 4(f)).

The plot of the coherence, evaluated along $\langle 001\rangle$ (C_{001}) and $\langle 1\bar{1}0\rangle$ ($C_{1\bar{1}0}$), versus T_S (figure 5(a)) represents in a quantitative way the ripple rotation shown in figure 4. For $T_S \leqslant 180$ K and $T_S \geqslant 340$ K no modulation is present on the surface ($C_{001} \cong C_{1\bar{1}0} \cong 0$), while in the intermediate-temperature range it is easy to distinguish two regions characterized by ripples with mutually perpendicular wave vectors: for $230 \leqslant T_S \leqslant 270$ K, $C_{001} \cong 0$ and $C_{1\bar{1}0} \cong 0.3$, while for $300 < T_S \leqslant 320$ K, $C_{0011} \cong 0.4$ and $C_{1\bar{1}0} \cong 0$. We also note that for $280\text{ K} \leqslant T_S \leqslant 300$ K the quite similar values of C_{001} and $C_{1\bar{1}0}$ indicate the coexistence of the two surface modulations.

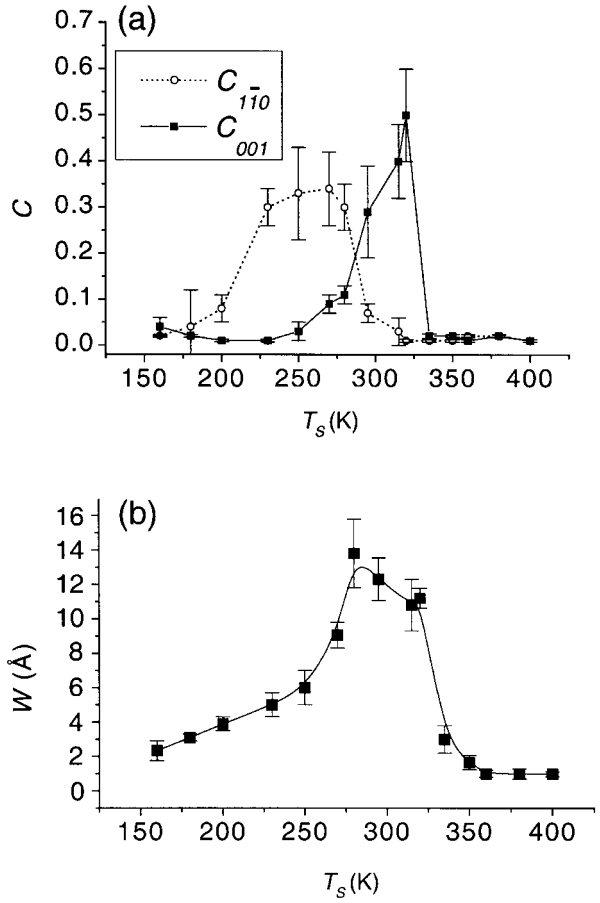

Figure 5. Surface coherence C along $\langle 001\rangle$ (C_{001}) and along $\langle 1\bar{1}0\rangle$ ($C_{1\bar{1}0}$) (a) and surface roughness W (b) as a function of the substrate temperature on Ag(110) after sputtering at $\Phi = 4\ \mu$A cm^{-2} and $t = 15$ min. To make it easier to understand the graphics, lines connecting the experimental points have been plotted to guide the eye.

Figure 5(b) shows the corresponding temperature evolution of the surface roughness. W does not decrease monotonically when the sputtering temperature is increased from $T_S = 180$ K to $T_S = 400$ K as one would have expected as a result of the increased adatom

diffusion and the consequent ability of the surface to erase ion damage: sample annealing is in fact regularly used to obtain smooth surfaces. On the contrary, $W(T_S)$ presents a peak near room temperature. Since the sputtering yield is almost temperature independent [21], at least over the temperature range analysed in the present work, both the roughness and the ripple orientation dependence on T_S indicate that the surface instability originates from diffusion processes and not, as it does for amorphous materials, from the surface-curvature-dependent erosion rate. The data reported in figures 4 and 5 show a general behaviour of the (110) surfaces of noble metals, since analogous results have been reported also for Cu(110) [14].

Ripple structures have not been observed on Ag(001) (figure 6). However, in this case also, the surface morphology is strongly dependent on the sputtering temperature T_S. In particular we can distinguish three temperature regimes. For $T_S \leqslant 200$ K small hills and holes

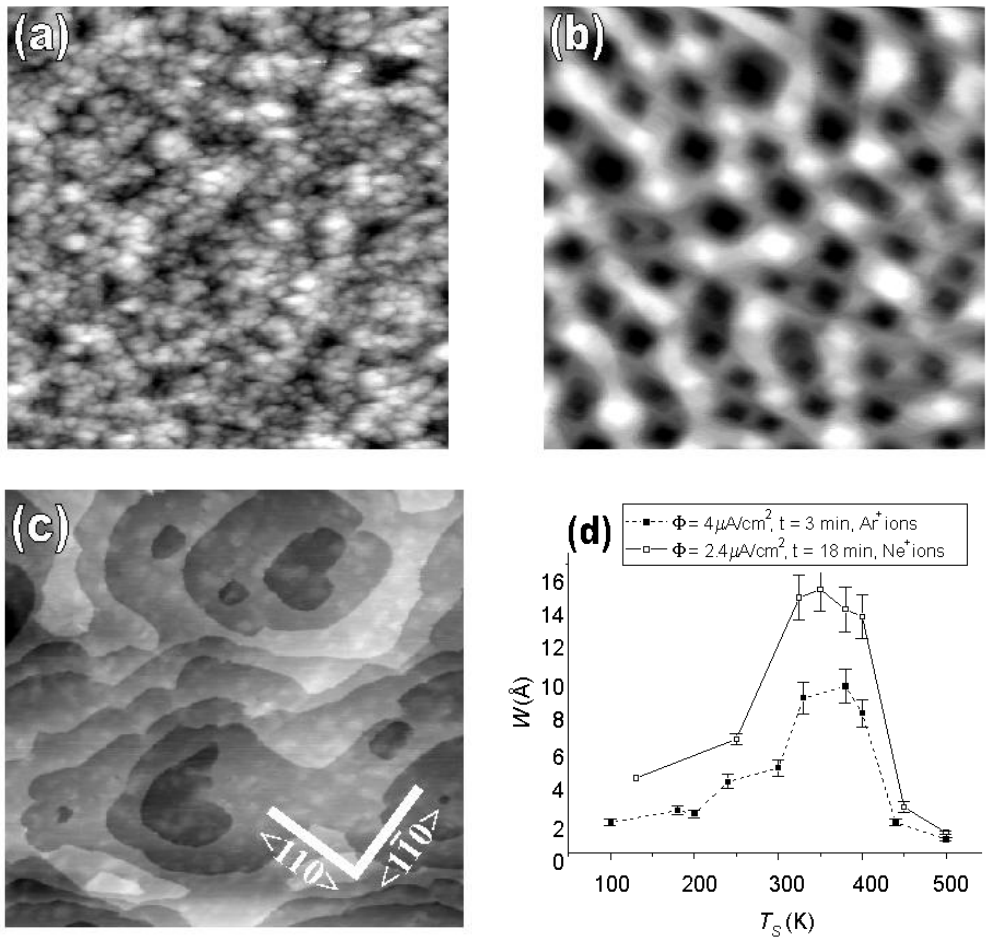

Figure 6. Temperature evolution of the Ag(001) surface morphology during ion sputtering. Images (a)–(c) refer to the experimental conditions $\Phi = 4\ \mu$A cm^{-2}, $t = 3$ min, Ar^+ ions. The sputtering temperatures T_S are: (a) $T_S = 130$ K; (b) $T_S = 350$ K; (c) $T_S = 450$ K. The image size is 120×120 nm^2 in (a), 290×290 nm^2 in (b) and 540×540 nm^2 in (c). In (d) the surface roughness W is shown as a function of the sputtering temperature T_S for two sets of experimental parameters: (filled squares) $\Phi = 4\ \mu$A cm^{-2}, $t = 3$ min, Ar^+ ions; and (open squares) $\Phi = 2.4\mu$A cm^{-2}, $t = 18$ min, Ne^+ ions.

a few layers deep are randomly distributed on the surface without any periodicity (figure 6(a)). The observed morphology is analogous to the one simulated in a random deposition model (chapter 4 in [22]) with a low value of W (figure 6(d)). When the substrate temperature is varied over the range 200 K $< T_S <$ 440 K, a quite regular pattern of square vacancy islands with a pyramid-like shape and well defined edges running along the $\langle 110 \rangle$ principal crystallographic directions is visible on the surface (figure 6(b)). Pit lateral dimension and separation are observed to be increasing functions of T_S [10]. In this temperature regime, W assumes high values with a maximum corresponding to $T_S \cong 350$ K. Finally, for $T_S \geqslant 440$ K, the surface becomes smoother (figure 6(c)) and again erosion takes place in a layer-by-layer fashion. In figure 6(d) the roughness data derived from these experiments are compared with data from a second series of sputtering experiments where Ne^+ ions have been used instead of Ar^+ ions. The two $W(T_S)$ curves have similar shapes, indicating that the observed temperature evolution does not depend on the details of the ion impact.

Keeping the value of T_S fixed and varying the ion flux, we can study the effect of the erosion rate on the final morphology. On Ag(110), figure 7(a) clearly shows a ripple rotation analogous to that observed on increasing the substrate temperature (compare with figure 4 and figure 5(a)). At the lowest fluxes considered ($\Phi \leqslant 4\mu$A cm^{-2}), a modulation with wave vector $\boldsymbol{k}$ along $\langle 001 \rangle$ is present on the surface ($C_{001} \cong 0.3$ and $C_{1\bar{1}0} \cong 0$) (figure 8(a)). In contrast, for $\Phi = 10$ μA cm^{-2} two waves are simultaneously observed, as demonstrated by $G(i, j)$, characterized by maxima in both the crystallographic directions (inset of figure 8(b)). At higher fluxes (14 μA cm$^{-2} \leqslant \Phi \leqslant 27$ μA cm^{-2}), the surface modulation with $\boldsymbol{k}$ along $\langle 001 \rangle$ vanishes ($C_{001} \cong 0$) while a ripple structure with $\boldsymbol{k}$ parallel to $\langle 1\bar{1}0 \rangle$ appears ($C_{1\bar{1}0} \cong 0.5$). The structure is thus rotated by 90° with respect to what is observed in the lower-flux regime (figure 8(c)). At the highest fluxes considered ($\Phi \geqslant 27$ μA cm^{-2}) the low value of C_{001} ($C_{001} \cong 0.1$) and the simultaneous reduction of $C_{1\bar{1}0}$ ($C_{1\bar{1}0} \cong 0.3$) indicate a degradation of the surface periodicity (figure 8(d)). Also on Ag(001), keeping the substrate temperature fixed, one can use the ion flux in order to change the coherence and the surface roughness. These data indicate that both substrate temperature and ion flux are parameters able to change the kinetics of the sputtering process.

5. Discussion

Ion sputtering is determined by atomic processes taking place within a finite penetration depth inside the bombarded substrate. The incoming ions penetrate into the surface and transfer their kinetic energy by colliding with the substrate atoms or inducing other types of process such as electronic excitations. As described by Sigmund's transport theory of sputtering [23], the energy deposition depth depends both on the microscopic structure of the substrate and on the characteristics of the impinging beam, i.e. the incidence angle and the ion energy. Following Sigmund's theory, Bradley and Harper [6] and, more recently, Cuerno and Barabasi [7] developed a continuum equation which describes the time evolution of the surface height h during sputtering erosion. Referring to the (x, y, h) laboratory frame, where h is the normal to the flat surface and ion trajectories are assumed to lie in the x–h plane (figure 2), this equation can be written as

$$\frac{\partial h}{\partial t} = -\nu_0 + \gamma \frac{\partial h}{\partial x} + \nu_x \frac{\partial^2 h}{\partial x^2} + \nu_y \frac{\partial^2 h}{\partial y^2} + \frac{\lambda_x}{2}\left(\frac{\partial h}{\partial x}\right)^2 + \frac{\lambda_y}{2}\left(\frac{\partial h}{\partial y}\right)^2 - D\,\nabla^2(\nabla^2 h) + |A(E,\theta)|\,\nabla^2 h + \eta \qquad (1)$$

where the coefficients γ, ν and λ depend on ion flux Φ, incidence angle θ and deposited energy distribution (see equation (4) in reference [7]). In particular ν_0 is the erosion rate

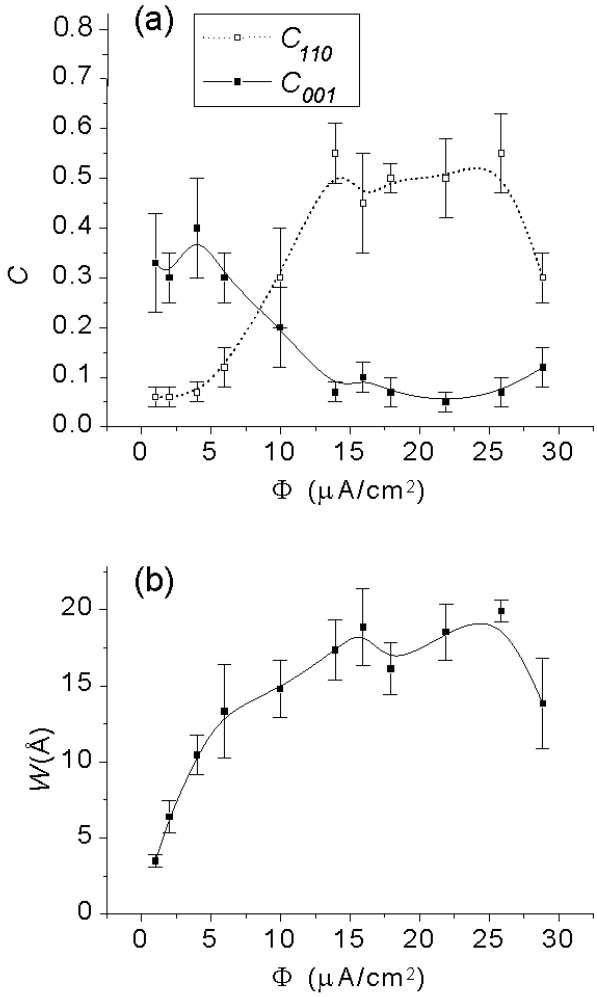

Figure 7. Flux dependences of C_{001}, $C_{1\bar{1}0}$ (a) and W (b) on Ag(110) ($T_S = 300$ K, $t = 20$ min). The connecting lines are plotted to guide the eye.

of the unperturbed planar surface, γ is the velocity of the in-plane motion of the surface structures [6] and the λ-coefficients determine the surface evolution on large length scales [7]. Coefficient D represents the surface diffusion constant induced by thermal diffusion and η is a white-noise term that accounts for the stochastic arrival of the ions. The most important aspect of equation (1) is that the surface evolution is mainly determined by the second-order-derivative terms [7]. In fact, while a Laplacian term with a positive coefficient has a stabilizing effect, the same term with a negative coefficient leads to a ripple-like instability whose origin is the faster erosion for the bottom of a trough than for the crest of a peak [6]. Thus, in equation (1), the competition between ν_x and ν_y determines the time evolution of the surface which, as experimentally observed on glass [1], silicon [3, 8] and Ge(001) [4], presents a periodic modulation with a wave vector $\boldsymbol{k}$ oriented along the direction (x or y) for which the ν-coefficient is negative and, in absolute value, the largest one. The smoothing term $|A(E, \theta)|\,\nabla^2 h$ has recently been proposed by Carter and Vishnyakov [8] in order to account

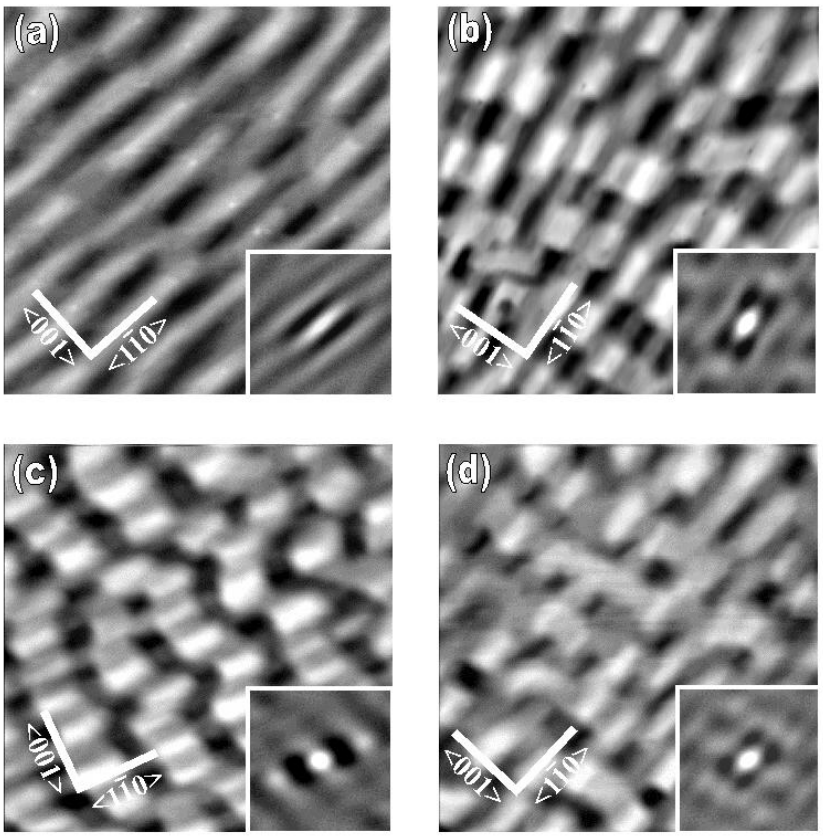

Figure 8. Four topographs (size 400 × 400 nm^2) illustrating the Ag(110) surface morphology after ion sputtering at $T_S = 300$ K and $t = 20$ min. The ion flux Φ is: (a) $\Phi = 4\ \mu$A cm^{-2}; (b) $\Phi = 10\ \mu$A cm^{-2}; (c) $\Phi = 16\ \mu$A cm^{-2}; (d) $\Phi = 29\ \mu$A cm^{-2}. The insets show enlargements of the corresponding $G(i, j)$ functions (area 250 × 250 nm^2).

for the effect of the recoiling-adatom diffusion induced by ion irradiation at a given energy E. For small values of θ, the positive coefficient $|A(E, \theta)|$ dominates ν_x and ν_y, thus overcoming the erosion instability and explaining the absence of the surface modulation observed on Si for near-to-normal ion incidence [8].

Equation (1), in spite of the good agreement with the experimental results on amorphous materials and semiconductors, is not able to explain the surface morphologies observed on single-crystal metals (see figures 4 and 6). For these systems, as pointed out by different authors [10–12, 14, 24], a more satisfactory model must entirely take into account both ion erosion and surface diffusion of the defects (adatoms and vacancies) created by ion sputtering. In our opinion, the discrepancy between experimental results and the forecasts of equation (1) is mainly due to an underestimation of the surface diffusion contribution. Some considerations lead us to this conclusion:

(1) Equation (1) does not predict any surface instability for normal sputtering whereas a lot of different morphological structures have actually been observed in this condition [9–14].
(2) While the ion damage is independent of the substrate temperature, at least in a first approximation [21], the observed evolution of the surface morphology is strictly connected

with the changes of T_S (figures 4 and 6).

(3) The diffusion term in (1) describes only an isotropic diffusion on a flat surface [25, 26] and does not take into account that the mobility of adatoms and vacancies on a single crystal is actually biased both in the vertical direction, by a Schwoebel barrier at the step edges, and in the surface plane. In fact, terrace diffusion takes place only along the principal crystallographic directions at rates that, as in the case of fcc (110) surfaces, may depend on the particular direction [14].

In order to take into account the peculiar properties of single-crystal metal surfaces and to explain the different morphologies observed on these systems, we suggest substituting for the term in (1) with a more general diffusion term. Limiting to the case of low-index surfaces, let us consider the two-dimensional vectors $\boldsymbol{n}$ that identify the principal crystallographic directions in the x–y surface plane. For each of these directions, we propose to add to equation (1) the two terms

$$-S_n(\boldsymbol{n}\cdot\boldsymbol{\nabla})^2 h - D_n(\boldsymbol{n}\cdot\boldsymbol{\nabla})^4 h \tag{2}$$

where S_n and D_n are positive coefficients that depend on the direction $\boldsymbol{n}$. The first term in (2) accounts for the asymmetry in the inter-layer diffusion due to step edge barriers [27, 29, 30] while the second one describes the diffusion on a flat terrace [25, 26, 28, 31]. In order to better clarify the role of these coefficients, let us consider the simple (but not always realistic) case in which the surface defects created by sputtering are single vacancies. Then S_n will depend on E_{S_n}, the vacancy Schwoebel barrier along $\boldsymbol{n}$, as $S_n \propto 1 - R_n$, where $R_n = \mathrm{e}^{-E_{S_n}/kT}$ is the ratio of the probability of hopping to a higher layer versus the probability of reflecting back on the terrace [27]. On the other hand, D_n will be proportional to the surface diffusivity, i.e. $D_n \propto \mathrm{e}^{-E_{D_n}/kT}$ where E_{D_n} is the energy barrier for vacancy diffusion along $\boldsymbol{n}$. More generally, the actual values of the coefficients S_n and D_n in equation (2) depend on the types of surface defect created during ion sputtering. In particular, recent single-impact experiments [32, 33] have shown that, in the case of metals, two kinds of defect are present, namely vacancy clusters and single or clustered adatoms. It is important to realize that, depending on the temperature, the diffusion of both of them may contribute to the final surface morphology and therefore that the correct contributions to equation (2) have to be considered for both kinds of defect.

5.1. Temperature evolution of the surface morphology

We first consider the Ag(110) surface which is characterized by two non-equivalent principal crystallographic directions, $\langle 001\rangle$ and $\langle 1\bar{1}0\rangle$ in the Miller indices notation. As a consequence, assuming for example $\langle 1\bar{1}0\rangle$ parallel to the x-axis, equation (2) becomes

$$-S_{001}\frac{\partial^2 h}{\partial x^2} - S_{1\bar{1}0}\frac{\partial^2 h}{\partial y^2} - D_{001}\frac{\partial^2 h}{\partial x^2} - D_{1\bar{1}0}\frac{\partial^2 h}{\partial y^2}. \tag{3}$$

The use of expression (3) together with the previously discussed smoothing term $|A(E,\theta)|\,\nabla^2 h$ suggested by Carter and Vishnyakov, allows us to write the linear approximation of equation (1) which, for *normal sputtering* ($\theta = 0^\circ$) of Ag(110), is

$$\frac{\partial h}{\partial t} = -\nu_0 + \gamma\frac{\partial h}{\partial x} + (\nu - S_{1\bar{1}0})\frac{\partial^2 h}{\partial x^2} + (\nu - S_{001})\frac{\partial^2 h}{\partial y^2} + |A(E,\theta)|\,\nabla^2 h$$
$$- D_{1\bar{1}0}\frac{\partial^4 h}{\partial x^4} - D_{001}\frac{\partial^4 h}{\partial y^4} + \eta \tag{4}$$

since, if $\theta = 0^\circ$, $\nu_x = \nu_y = \nu$ [7]. Neglecting the non-linear terms in equation (1) is a first approximation which suffices for the purposes of the present paper. In fact the non-linear

terms only affect the spatial scaling laws of the surface on long length scales, while the linear ones define whether or not the surface is unstable over short length scales [7]. In particular, as previously observed, the surface morphology is determined by the competition among the three Laplacian terms, i.e. the two roughening coefficients, $\nu - S_{1\bar{1}0}$ and $\nu - S_{001}$, and the smoothing one $|A(E,\theta)|$. Since the S-coefficients, unlike ν and A, are temperature dependent, T_S determines which one dominates among the three. In order to directly derive from equation (4) the surface morphology evolution as a function of T_S, one needs to write out explicitly the expression for the coefficients which appear in (4). On the other hand, depending on the particular type of surface defect, S and D may have a very complex form since they describe the concerted motion of vacancies and adatoms involving a large number of different microscopic processes. As a consequence, in the following we will limit ourselves to inferring the mutual relations between these coefficients from our experimental data, leaving their exact evaluation to more expert theoreticians. Nevertheless a general point can be made: whatever the exact expression for S_n is, its destabilizing effect on the surface morphology will be effective only if it describes an uphill current of surface defects, which means that (a) surface defects are actually moving along direction $\boldsymbol{n}$ and (b) surface defects bounce back at step edges, i.e. they do not have enough energy for inter-layer diffusion.

At the lowest temperature considered ($T_S = 180$ K), the experimental data in figure 4(a) show a non-periodic surface ($C_{001} \cong C_{1\bar{1}0} \cong 0$) characterized by a low value of W ($\approx$4 atomic layers), indicating that the diffusion of surface defects is too low for the creation of organized surface structures and thus showing a predominance of the smoothing coefficient. For $T_S = 230$ K, the higher thermal energy leads to an increase in the number of moving surface defects. Nevertheless, terrace diffusion takes place almost only in the in-channel direction, because of the difference in the migration energy barriers for $\langle 1\bar{1}0\rangle$ and $\langle 100\rangle$, and the inter-layer motion is still forbidden. In fact, the probability of crossing a step edge is already low for adatoms (see [17] for adatom-diffusion energy barriers on Ag(110)), implying that less mobile surface defects, such as vacancies and clusters, almost always bounce back when approaching step edges. This situation generates a destabilizing uphill current parallel to $\langle 1\bar{1}0\rangle$ which, in the continuum equation, is represented by the predominance of the coefficient $\nu - S_{1\bar{1}0}$. The effects on the surface morphology are clearly shown by the rippled structure with the $\boldsymbol{k}$-vector along $\langle 1\bar{1}0\rangle$ (ridges along $\langle 001\rangle$) that can be seen in figure 4(b). The rectangular mounds that appear at higher temperatures ($280 \leqslant T_S \leqslant 300$ K; figure 4(c)), can be interpreted as resulting from the superposition of two perpendicular ripple instabilities with different wavelengths. In equation (4) this is represented by an increased magnitude of the roughening coefficient $\nu - S_{001}$ which becomes comparable with $\nu - S_{1\bar{1}0}$, and can be explained by a temperature-induced increase in the $\langle 001\rangle$ diffusion of surface defects. The further evolution of the surface with T_S shows a gradual attenuation of the $\langle 1\bar{1}0\rangle$ instability (figure 4(d)) up to the point where only ripples with $\boldsymbol{k}$ parallel to $\langle 001\rangle$ are left (figure 4(e)). This is a clear indication that, in the 300–320 K range, $S_{1\bar{1}0}$ is reduced with respect to S_{001} because of the increased thermal energy of sputtering-induced defects which begin to descend steps in the $\langle 1\bar{1}0\rangle$ direction and thus do not contribute to the corresponding uphill current. On the other hand, the higher step edge energy barriers still forbid inter-layer diffusion along $\langle 001\rangle$ and thus a destabilizing uphill current is still present along $\langle 001\rangle$, producing the observed ripples with a $\langle 001\rangle$-oriented wave vector. Finally, for $T_S \geqslant 340$ K, inter-layer motion is active along both crystallographic directions and therefore both destabilizing coefficients S get smaller, while the smoothing effect of the fourth-order terms in (4) prevails (figure 4(f)).

A similar analysis in terms of the continuum equation (1) can also be done for the temperature evolution of the square-symmetry surface Ag(001). In this case the two principal crystallographic directions $\langle 110\rangle$ and $\langle 1\bar{1}0\rangle$ are equivalent, implying that the relations $D_{110} =$

$D_{1\bar{1}0} = D$ and $S_{110} = S_{1\bar{1}0} = S$ hold for the diffusion coefficients introduced in (2). Therefore, taking for simplicity $\langle 110 \rangle$ parallel to the x-axis, the linear approximation of equation (1) for Ag(001) becomes

$$\frac{\partial h}{\partial t} = -\nu_0 + \gamma \frac{\partial h}{\partial x} + (\nu - S)\,\nabla^2 h + |A(E,\theta)|\,\nabla^2 h - D\frac{\partial^4 h}{\partial x^4} - D\frac{\partial^4 h}{\partial y^4} + \eta. \tag{5}$$

In terms of the diffusivity of sputter-induced surface defects, the square symmetry of the substrate implies that whenever the defect thermal energy is the right one for the creation of a periodic ripple structure with wavelength λ along one of the two directions, an equivalent instability, with the same λ, is also produced in the perpendicular orientation. As a consequence, the only structures that can be formed by normal-incidence sputtering on Ag(001) are ensembles of square symmetric pits and mounds deriving from the superposition of two identical and perpendicular rippled surface undulations. Note that this result can also be formally derived from the solutions of equation (5).

Before continuing with the temperature-dependent analysis of equation (5), we observe that recently some of us [33] gave a thorough description of the morphological evolution of a sputtered Ag(001) surface by recognizing the exact types of surface defect created by sputtering (small adatom and vacancy clusters) and by analysing their temperature-dependent diffusion. In the present work, we want to approach the same problem from a less detailed point of view, not distinguishing among the different types of sputter-induced surface defect and being mainly interested in their intra- and inter-layer mobility. As a consequence, we can identify three main temperature regimes. For $T_S \leqslant 200$ K the defect mobility is low, so the diffusion instabilities cannot grow and the morphology is determined by the smoothing term that overcomes the erosion instability induced by ν (figure 6(a)). For 200 K $\leqslant T_S < 440$ K the intra-layer diffusion is activated, but the step edge barriers still prevent inter-layer motion. The simultaneous operation of these two conditions induces the formation of surface structures which, from the arguments given above, appear as the pattern of square holes and mounds shown in figure 6(b). For $T_S \geqslant 440$ K the defect thermal energy is large enough to overcome the step edge barriers and thus the smoothing effect of the fourth-order derivative terms in (5) dominates the surface evolution (figure 6(c)).

5.2. Flux evolution of the surface morphology

In the case of Ag(110), we studied the dependence of the roughness W and the surface coherences C_{001} and $C_{1\bar{1}0}$ on the ion flux Φ, keeping the substrate temperature fixed at 300 K. At this T_S, the two diffusion instabilities are simultaneously present on the surface (see section 5.1) and the roughness is at its maximum (figure 5(b)), so the effect of the ion erosion rate on the surface morphology can be easily detected. A comparison between figure 5(a) and figure 7(a) clearly shows that a flux increase generates a 90° rotation of the surface periodicity direction, similar to that observed on lowering the substrate temperature.

A comparison with growth experiments can help us to understand this effect. In fact, a similar relation between flux and temperature dependence is observed in the sub-monolayer growth regime. Experimental results [22, 34–36] and computer simulations [37–41] show that the density of islands created during deposition can be increased by lowering the deposition temperature or by increasing the adatom flux, as a consequence of the reduced area described by each single adatom before it nucleates. In the case of a sputtering process, the framework is quite similar. In fact, in the previous sections we have shown that periodic structures grow only if defects produced by the random ion bombardment can diffuse generating a coherent reorganization of the surface. Following a simplifying picture, we note that the area L^2 visited

by a surface defect in the time interval Δt between two successive ion impacts on the same area depends on the ion flux Φ as $L^2 = e/(\Phi\,\Delta t)$, with e the electron charge. If one assumes that the defect carries out a random walk, this area can also be expressed as $L^2 = \Gamma\,\Delta t$, where Γ is the surface diffusivity. Therefore $L^2 = \sqrt{e\Gamma/\Phi}$, which means that the ability a defect has to redistribute itself on the surface decreases in the same way by increasing Φ or by lowering the substrate temperature. For this reason, at very high fluxes, surface reorganization should be completely inhibited and the surface should be rough without any evidence of periodic structures. Although our experimental set-up does not allow us to get ion fluxes larger than 30 μA cm^{-2}, the decrease of $C_{1\bar{1}0}$ for $\Phi \geqslant 27$ μA cm^{-2} in figure 7(a) suggests that such a regime is setting in. A similar conclusion is also supported by the behaviour of W which increases for low values of Φ, reaches a saturation value and finally, at the highest values of Φ considered, starts to decrease (figure 7(b)), indicating a predominance of the irradiation effects on the instability due to surface diffusion.

We are not able to determine the explicit dependence on Φ of the coefficients in equation (4). However we think that the major dependence has to be contained in the D-coefficients. In fact, as we have already pointed out, the presence of a Schwoebel barrier that limits the inter-layer diffusion (S-terms) is only a necessary condition for a surface instability arising, and is not a sufficient one. Sputter-induced defects have to move on the surface and to reach a step in order to feel its effect. This information is contained in the coefficients D_{001} and $D_{1\bar{1}0}$ that indicate whether and in what direction diffusion is activated.

Similarly, we also investigated the effect of the ion erosion rate on the surface morphology in the case of Ag(001). For this surface we chose a substrate temperature $T_S = 380$ K, corresponding to the observed maximum of W in figure 6. The experimental data are consistent with an increase of the coherence and the roughness with Φ, until for $\Phi \geqslant 10$ μA cm^{-2}, saturation values are reached. Even if in this case we are not able to detect the reduction of roughness and coherence that we observed on Ag(110) at the highest examined fluxes, the data confirm that ion sputtering is a complex process determined by the competition between erosion and diffusion. In this framework both ion flux and substrate temperature are macroscopic parameters that can be varied in order to give prominence to diffusion or erosion effects.

6. Summary and conclusions

In this work, we studied the effect of normal-incidence ion sputtering on single-crystal metals. The experimental data show that ion bombardment on Ag(110) produces a ripple structure whose wave vector, depending on substrate temperature and ion flux, is directed along $\langle 001\rangle$ or $\langle 1\bar{1}0\rangle$. In similar experimental conditions, ion sputtering on a square-symmetry surface, such as Ag(001), produces a periodic pattern of square holes with edges parallel to the crystallographic directions. We have discussed how these structures derive from surface instabilities that originate not from the surface-curvature-dependent erosion (as in the case of amorphous and semiconductor materials), but from diffusion processes which play a leading role in determining the surface evolution. Ion sputtering is a kinetic process in which the erosion rate, i.e. the impinging ion flux, fixes the timescale, while the energy activation barriers establish a hierarchy among the different diffusion processes that redistribute the defects produced by each ion impact. In this framework, both the substrate temperature and the ion flux can be used to select and enhance only certain diffusion processes and consequently to tune the final surface morphology. In particular, on an anisotropic surface, such as Ag(110), they select in which of the two crystallographic directions the inter-layer mobility is inhibited, leading to the growth of two different and perpendicular ripple structures, while on an isotropic surface, such as Ag(001), temperature and ion flux only determine whether or not the diffusion instability

is active.

These effects are included in a continuum equation (equation (4)) which is an extension of the models introduced by Bradley and Harper [6] and Cuerno and Barabasi [7] and is sufficiently general to be applied to different surfaces. For substrates with high energy diffusion barriers, such as amorphous materials, or equivalently in the low-temperature regime, equation (4) reduces to those previous models [6, 7]. In contrast, for surfaces on which diffusion is activated, such as single-crystal metals, it can be used to describe the periodic structures observed both on isotropic and anisotropic substrates.

Acknowledgments

We thank M Rost and T Ala-Nissila for helpful correspondence and discussions.

References

[1] Navez M, Sella C and Chaperot D 1962 *C. R. Acad. Sci., Paris* **254** 240
[2] Mayer T M, Chason E and Howard A J 1994 *J. Appl. Phys.* **76** 1633
[3] Lewis G W, Nobes M J, Carter G and Whitton J L 1980 *Nucl. Instrum. Methods* **170** 363
[4] Chason E, Mayer T M, Kellerman B K, McIlroy D T and Howard A J 1994 *Phys. Rev. Lett.* **72** 3040
[5] Vajo J J, Doty R E and Cirlin E 1996 *J. Vac. Sci. Technol.* A **14** 2709
[6] Bradley R M and Harper J M E 1988 *J. Vac. Sci. Technol.* A **6** 2390
[7] Cuerno R and Barabasi A L 1995 *Phys. Rev. Lett.* **74** 4746
[8] Carter G and Vishnyakov V 1996 *Phys. Rev.* B **54** 17 647
[9] Ritter M, Stindtmann M, Farle M and Baberschke K 1996 *Surf. Sci.* **348** 243
[10] Costantini G, Rusponi S, Gianotti R, Boragno C and Valbusa U 1998 *Surf. Sci.* **416** 245
[11] Michely T and Comsa G 1993 *Nucl. Instrum. Methods* B **82** 207
[12] Murty R M V, Curcic T, Judy A, Cooper B H, Woll A R, Brock J D, Kycia S and Headrick R L 1998 *Phys. Rev. Lett.* **80** 4713
[13] Naumann J, Osing J, Quinn A J and Shvets I V 1997 *Surf. Sci.* **388** 212
[14] Rusponi S, Costantini G, Boragno C and Valbusa U 1998 *Phys. Rev. Lett.* **81** 2735
[15] Conti R, Rusponi S, Pagnotta D, Boragno C and Valbusa U 1997 *Vacuum* **48** 639
[16] Rusponi S, Boragno C and Valbusa U 1997 *Phys. Rev. Lett.* **78** 2795
[17] Hontinfinde F, Ferrando R and Levi A C 1996 *Surf. Sci.* **366** 306
[18] Koponen I, Hautala M and Sievanen O-P 1997 *Phys. Rev. Lett.* **78** 2612
[19] Maunuksela J, Myllys M, Kahkonen O P, Timonen J, Provatas N, Alava M J and Ala-Nissila T 1997 *Phys. Rev. Lett.* **79** 1515
[20] Yang H N, Zhao Y P, Chan A, Lu T M and Wang G C 1997 *Phys. Rev.* B **56** 4224
[21] Roosendal H E 1981 *Sputtering by Particle Bombardment* ed R Behrisch (Heidelberg: Springer)
[22] Barabasi A L and Stanley H E 1995 *Fractal Concepts in Surface Growth* (Cambridge: Cambridge University Press)
[23] Sigmund P 1969 *Phys. Rev.* **184** 383
[24] Rusponi S, Costantini G, Boragno C and Valbusa U 1998 *Phys. Rev. Lett.* **81** 4184
[25] Lai Z W and Das Sarma S 1991 *Phys. Rev. Lett.* **66** 2348
[26] Wolf D E and Villain J 1990 *Europhys. Lett.* **13** 389
[27] Johnson M D, Orme C, Hunt A W, Graff D, Sudijomo J, Sander L M and Orr B G 1994 *Phys. Rev. Lett.* **72** 116
[28] Makeev M A and Barabasi A L 1997 *Appl. Phys. Lett.* **71** 2800
[29] Krug J, Plischke M and Siegert M 1993 *Phys. Rev. Lett.* **70** 3271
[30] Siegert M and Plischke M 1994 *Phys. Rev. Lett.* **73** 1517
[31] Herring C 1950 *J. Appl. Phys.* **21** 301
[32] Morgenstern M, Michely T and Comsa G 1999 *Phil. Mag.* A **79** 775
[33] Costantini G, Buatier de Mongeot F, Boragno C and Valbusa U 2001 *Phys. Rev. Lett.* **86** 838
[34] Ernst H-J, Fabre F and Lapujoulade J 1992 *Phys. Rev.* B **46** 1929
[35] Zuo J-K, Wendelken J F, Durr H and Liu C-L 1994 *Phys. Rev. Lett.* **72** 3064
[36] Roder H, Hahn E, Brune H, Bucher J P and Kern K 1993 *Nature* **366** 141
[37] Bartelt M C, Tringides M C and Evans J W 1993 *Phys. Rev.* B **47** 13 891

[38] Bartelt M C and Evans J W 1992 *Phys. Rev.* B **46** 12 675
[39] Bartelt M C, Perkins L S and Evans J W 1995 *Surf. Sci.* **344** L1193
[40] Ratsch C, Zangwill A, Smilauer P and Vvedensky D D 1994 *Phys. Rev. Lett.* **72** 3194
[41] Ratsch C, Smilauer P, Zangwill A and Vvedensky D D 1995 *Surf. Sci.* **329** L599